

Battery-Dynamics Driven TDMA MAC Protocols for Wireless Body-Area Monitoring Networks in Healthcare Applications

Hang Su, *Student Member, IEEE*, and Xi Zhang, *Senior Member, IEEE*

Abstract—We propose the cross-layer based battery-aware time division multiple access (TDMA) medium access control (MAC) protocols for wireless body-area monitoring networks in wireless healthcare applications. By taking into account the joint effect of electrochemical properties of the battery, time-varying wireless fading channels, and packet queuing characteristics, our proposed schemes are designed to prolong the battery lifespan of the wireless sensor nodes while guaranteeing the reliable and timely message delivery, which is critically important for the patient monitoring networks. In addition, we develop a Markov chain model to analyze the performance of our proposed schemes. Both the obtained analytical and simulation results show that our proposed schemes can significantly increase the battery lifespan of sensor nodes while satisfying the reliability and delay-bound quality of service (QoS) requirements for wireless body-area monitoring networks. Furthermore, the case study of the electrocardiogram (ECG) monitoring application shows that besides meeting the delay requirements, our proposed schemes outperform the IEEE 802.15.4 and Bluetooth protocols in terms of battery lifespan.

Index Terms—Battery-dynamics model, cross-layer design, queuing model, wireless body-area networks, wireless healthcare applications.

I. INTRODUCTION

BASED on the state-of-the-art wireless communications/networks and the advanced biomedical material technologies, wireless telemedicine systems emerge as a promising solution to the challenge of recently higher and higher health care expenses. One of the most important areas in the wireless telemedicine system is monitoring of patients and intervention from health care professionals when required. This will reduce the total health care cost, resulting in a better utilization of limited health care resources. It also enables independent living for increasingly older individuals, especially in the countries with large portion of aging population. Using the new generation of biomedical material technology, the wireless telemedicine with biomedical sensors offers a large amount of opportunities that allow new measurements and monitors on human and new approaches for diagnosis. The implanted and wearable non-invasive sensors are able

to measure a large number of vital body parameters such as electrocardiogram (ECG), pulse, blood oxygen saturation, skin temperature, blood pressure, hemodynamic calculator, etc. [1].

The biomedical sensors benefit from significant advances in system integration and can be applied in different body locations. However, such implanted or wearable devices can cover only a specific and generally a small body measurement area and cannot fulfill alone all the needs for displaying, interacting with the user and communicating. All the sensor devices are required to communicate with a wearable or near-body coordinator, which collects and processes the data from the sensors. The coordinator analyzes the collected data locally or transmits the aggregated data to the gateway of the Internet which is connected with the hospital monitoring networks. Thus, a typical wireless body-area monitoring network is composed of a number of wireless sensor devices and a coordinator, as shown in Fig. 1, which depicts the large picture of the wireless patient monitoring networks.

The implanted and wearable sensor devices are typically powered by *batteries* that have only limited energy capacity. The advances in battery technology are much slower than the recent advances that have taken place in the field of wireless communications and networks. At the same time, due to potentially life-threatening situations, the reliable and timely delivery of vital body parameters is the more critical requirement of patient monitoring. Hence, how to efficiently utilize the limited battery energy of sensor nodes and thus prolong the lifetime of the sensor devices, while guaranteeing the reliability and timely message delivery is the most crucial goals for the design of wireless patient monitoring networks. It is well known that the radio transceiver is the most energy-consumption component of sensor nodes. Thus, the design of energy-efficient MAC protocols is the main challenge in designing for wireless body-area monitoring networks.

To tackle the above mentioned challenges, we propose and analyze the cross-layer design based battery-aware time division multiple access (TDMA) medium access control (MAC) protocols for wireless body-area monitoring networks, which takes the battery discharge dynamics, wireless channel models, short transmission ranges, and queuing characteristics into consideration. The objective of our proposed schemes is to maximize the life-span and battery utilization of the wireless sensor nodes while satisfying the delay-bound quality of service (QoS) requirements for the wireless body-area monitoring networks. The key of our proposed schemes is

Manuscript received 15 July 2008; revised 13 February 2009. The research reported in this paper was supported in part by the National Science Foundation CAREER Award under Grant ECS-0348694.

The authors are with the Networking and Information Systems Laboratory, Department of Electrical and Computer Engineering, Texas A&M University, College Station, TX 77843 USA (e-mails: hangsu@ece.tamu.edu; xizhang@ece.tamu.edu).

Digital Object Identifier 10.1109/JSAC.2009.090507.

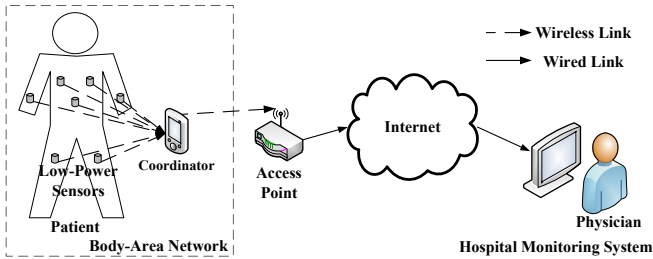


Fig. 1. The wireless patient monitoring networks.

to best utilize and adapt to the electrochemical properties of batteries and the time-varying characteristics of wireless fading channels together. To characterize and analyze our proposed scheme, we also develop a discrete time Markov chain for the performance evaluations. Using our proposed schemes, the analytical and simulation results show significant improvement in the battery lifespan while the delay QoS requirement specified by wireless patient monitoring networks is still guaranteed.

The rest of this paper is organized as follows. Section II discusses the related works. Section III describes the system models. Section IV proposes our battery-aware TDMA scheduling based MAC protocols. Section V develops the Markov chain based model to analyze the performance of our proposed schemes. Section VI evaluates our proposed schemes by using our developed Markov chain model and simulation experiments. The paper concludes with Section VII.

II. RELATED WORKS

A large number of the energy-efficient packet transmission scheduling schemes in the data link layer have been proposed for wireless sensor networks in recent years [2]–[5]. The authors of [2] developed a round-robin scheduling scheme to evenly discharge multiple battery cells. The authors of [3] proposed a contention based medium access control (MAC) protocol which exploits the battery dynamics to increase network lifetime. In [4], the authors proposed a cluster-based TDMA protocol. It adapts the frame period to the user traffic such that idle sensor nodes can power off the radio to save power. The authors of [5] proposed a TDMA-based multiple-hop MAC protocol for large-scale wireless sensor networks. However, none of the existing work takes into account the joint effect of battery dynamics, wireless fading channels at the physical layer, and queuing management at the data link layer, which has immediate and significant effects on the lifespan of sensor nodes.

IEEE 802.15.4 [6], which is specifically devised to support low power and low data rate networks, is considered as the promising MAC protocol for large-scale wireless sensor networks [7]. The IEEE 802.15.4 with beacon mode supports two types of medium access modes, such as TDMA-based contention free period (CFP) mode and carrier sense multiple access with collision avoidance (CSMA/CA)-based contention access period (CAP) mode. The CFP mode of IEEE 802.15.4 is basically the same as the standard TDMA scheme which is a special case of our proposed schemes. On the other hand, Bluetooth [8], [9] is another alternative MAC protocol for low

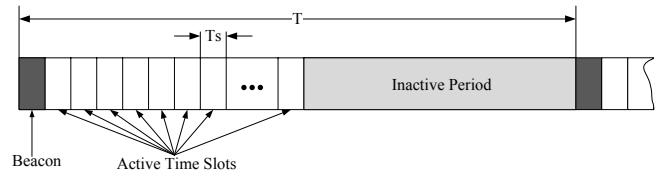


Fig. 2. TDMA frame structure.

cost and low power wireless personal area network. In the piconet mode of the Bluetooth protocol, there are up to 7 slave devices and 1 master device. The communications between the slave devices and master device is based on TDMA scheduling. The master device defines the time slot assignments. The Bluetooth protocol with piconet is essentially the same as the standard TDMA scheme.

III. SYSTEM MODELS

A. Basic Framework

We concentrate on the wireless body-area monitoring networks as shown in Fig. 1. In particular, we are mainly interested in part of the data gathering process from the low-power sensors to the powerful coordinator in this paper. More specifically, the sensor nodes, each of which is powered by a battery with *limited* capacity, communicate with the coordinator by using a single-transmit and a single-receive antenna. The sensor nodes transmit the sensed information at a constant power to their coordinator in a time-division manner, i.e., based on the TDMA scheduling. The time axis is divided into periodical frame periods, each of which consists of three parts, including the beacon slot, the active time slots, and the inactive period, as shown in Fig. 2. The length of the frame period is adaptive to the requirements of the applications.

In the beacon slot, the coordinator broadcasts the beacon signal, which is used to indicate the length of the frame period and help estimate the channel state information (CSI). The sensor nodes having packets to send wake up at the beginning of the beacon slot. In the frame period, each active time slot with a length of T_s is owned by a distinct sensor node. According to the packet scheduling schemes and wireless channel condition, the sensor nodes decide whether or not to utilize the channel at different frame periods. During the inactive period, no data is exchanged between the sensor nodes and the coordinator. To efficiently save the energy, each sensor node is active during the beacon slot and its own time slot only when it has packets to send. Otherwise, it is in the sleep state.

B. The Battery Discharge Dynamics

Chiasserini and Rao in [10], [11] studied the battery discharge dynamics and showed that the batteries are capable of recovering the initial value of voltage when they remain idle for a certain period, which is the so-called battery's recovery capacity effect. The recovery process depends on the idle time duration and the charge state of the batteries. In particular, as the battery is discharged, the recovery capability decreases until all the active materials that react electrochemically to produce electrical energy are consumed.

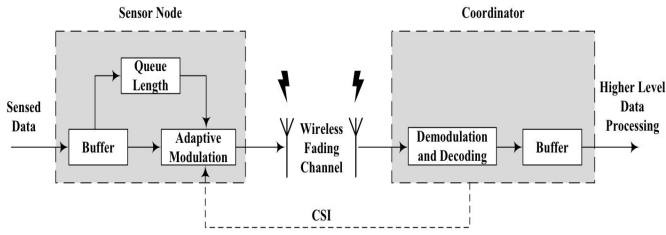


Fig. 3. The diagram of the system architecture for our proposed schemes.

A battery can be characterized by the theoretical capacity and nominal capacity. The theoretical capacity of batteries is decided by the amount of active materials contained in the cell and is expressed in terms of ampere-hours. The total number of discharges cannot exceed the battery's theoretical capacity. The nominal capacity of the batteries is defined as the capacity actually available when the battery is discharged at a specific constant current. Due to the battery's recovery capacity effect, the nominal capacity may probably increase when the battery remains idle for a specific period of time. Suppose that the amount of capacity necessary to transmit packets during a time slot is one unit of the charge. We set the theoretical capacity to be E_T charge units and the nominal capacity to be E_N charge units. Let E_R ($E_R < E_N$) be the remaining battery capacity. Following the battery discharge model proposed in [11], the dynamics of the batteries can be described as follows: i) If the sensor node sends packets during a time slot, one unit of the charge is consumed; ii) If the sensor node remains idle during a period of time, the battery can recover one unit of the charge at a probability of $e^{-c(E_N - E_R)}$, where c is a real-valued number depending on the battery's electrochemical properties. The smaller the value of c , the larger the recovery capability.

C. The Wireless Channel Model

Suppose that the wireless link between the sensor nodes and the coordinator has the symmetric channel gain and is characterized by a slow flat fading channel. The channel state remains unchanged during each frame period, but varies from frame period to frame period. The channel state can be characterized by the received signal-to-noise ratio (SNR), denoted by γ . The general Nakagami- m model [12] has been shown to be able to accurately describe the fading characteristics of the wireless body-area networks [13]. Hence, we use the Nakagami- m model, with the average received SNR $\bar{\gamma} = E[\gamma]$, to model the wireless fading channel in this paper. Under the Nakagami- m model, the probability density function of the received SNR (γ) is given by

$$p_\gamma(\gamma) = \frac{1}{\gamma \Gamma(m)} \left(\frac{m\gamma}{\bar{\gamma}} \right)^m e^{-\frac{m\gamma}{\bar{\gamma}}}, \quad (1)$$

where m , ($m \geq 1/2$) is the Nakagami fading parameter and $\Gamma(x) = \int_0^\infty t^{x-1} e^{-t} dt$ is the Gamma function. The Nakagami- m model can embrace various types of wireless fading channels. For example, Rayleigh channel is a special case of Nakagami- m model when $m = 1$. Furthermore, the Rician fading channels can be approximated by the Nakagami-

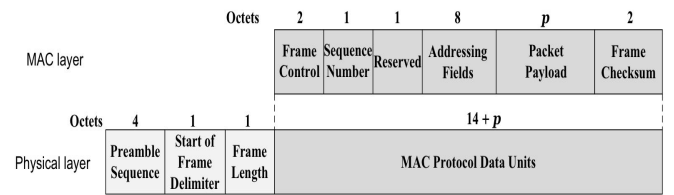


Fig. 4. The structure of a data packet.

m model by a one-to-one mapping between the Nakagami fading parameter m and the Rician factor [12].

IV. OUR PROPOSED SCHEMES

A. Protocol Overview

Based on the battery's recovery capacity effect, it is reasonable to expect that the battery can yield a longer lifespan if it has more rest time between two consecutive discharge states. Thus, we propose the battery-aware TDMA scheduling based MAC protocols, which aim at maximizing the idle periods for the batteries of sensor nodes while satisfying the delay-QoS requirements. Our proposed schemes take into account the joint effect of the battery dynamics, the wireless-channel qualities at the physical layer, and queuing characteristics at the data link layer. The key idea of our proposed schemes is to make the sensor nodes to efficiently utilize the time slots. Particularly, in our proposed schemes, the sensor nodes may hold the packets until there are sufficient packets available and the channel is in good state. In other words, the sensor nodes transmit the packets in the buffer only if the channel is good and the buffer size is large enough. In this way, the number of idle time slots may increase, which enables the battery to recover capacity and thus prolongs the lifespan of the sensor node. On the other hand, holding more packets in the buffer introduces larger packet delay and packet drop rate of the sensor nodes, which clearly imposes a tradeoff between the battery lifetime span and packet delay and loss QoS requirements.

The system architecture of our proposed schemes is shown in Fig. 3, where a finite-length first-in-first-out (FIFO) queue/buffer is employed at the sensor nodes. If the buffer is full, the new arriving packets will be dropped. The packets queuing through the buffer are processed at the adaptive modulation module, and then transmitted through the antenna. The objective of adaptive modulation is to maximize the data rate by adjusting transmission parameters to the available CSI, while maintaining a predetermined bit error rate. The sensor nodes estimate CSI by analyzing the signal strength of the beacon frame received from the coordinator at the beginning of each frame period. The received CSI and the queue length information of the buffer are used together to control the adaptive modulation module in deciding the data rate for packet transmissions. Fig. 4 illustrates the structure of a data packet. The packet's signaling overhead is 20 bytes including 6 bytes at physical layer and 14 bytes at MAC layer. Denote by p the length of packet payload.

We introduce three parameters: θ_a , θ_b , and θ_c to achieve the desirable tradeoff between the idle probability of time slots and packet delay as well as packet drop rate. In our proposed

Algorithm 1 Our proposed TDMA scheduling based MAC protocols

For each sensor node in its assigned time slot of the t -th frame period

01. estimate the CSI by analyzing the beacon packet
02. $n :=$ number of packets in the buffer
03. $m :=$ estimated number of pkts it can transmit based on the CSI
04. **if** $n > \theta_c$ or $(m > \theta_a$ and $n > \theta_b)$
05. transmit packets in the buffer
06. **else**
07. hold packets in the buffer
08. **end**

Fig. 5. Pseudo code of our proposed schemes.

schemes, at the beginning of each frame period, each sensor node estimates the number of packets that can be transmitted during this frame period. When the queue size is no larger than θ_c , the sensor nodes avoid transmitting packets if the estimated number of packets that can be transmitted is less than θ_a or the queue size is smaller than θ_b , where $\theta_c > \max\{\theta_a, \theta_b\}$. Note that the standard TDMA scheme is a special case of our proposed schemes when $\theta_a = \theta_b = 1$ and it provisions the most stringent delay QoS-requirements for the sensor nodes. The objective of θ_c is to make our proposed schemes to work as the standard TDMA scheme when the buffer size is large. Algorithm 1 given in Fig. 5 shows the pseudo code for our proposed schemes. As we can predict, the larger the values of θ_a and θ_b are, the higher the packet delay, packet drop rate, and idle probability of time slots are. In Sections V and VI, we will detail how to balance the tradeoff between battery lifespan and packet delay by tuning up these parameters through analytical models and simulations.

V. ANALYTICAL MODELS

A. Adaptive Modulation

Consider the adaptive modulation module which adopts the M -ary square QAM and $M = I \times J$ rectangular QAM. Note that for M -ary square QAM, $I = J = \sqrt{M}$. The bit error rate (BER) of M -ary QAM is given by [14]:

$$P_b^{I,J}(\gamma) = \frac{1}{\log_2 M} \left(\sum_{i=1}^{\log_2 I} Z(i, I) + \sum_{j=1}^{\log_2 J} Z(j, J) \right), \quad (2)$$

where $Z(k, x)$ is the probability that the k th bit in x (in-phase or quadrature) component is error and x can be equal to I or J . $Z(k, x)$ can be expressed as:

$$Z(k, x) = \frac{1}{x} \sum_{i=0}^{(1-2^{-k})x-1} \left\{ \operatorname{erfc} \left((2i+1) \left(\frac{3\gamma \log_2 M}{I^2 + J^2 - 2} \right)^{\frac{1}{2}} \right) \right. \\ \left. (-1)^{\lfloor \frac{i2^k-1}{x} \rfloor} \left[2^{k-1} - \left\lfloor \frac{i2^k-1}{x} + 0.5 \right\rfloor \right] \right\}, \quad (3)$$

where $\operatorname{erfc}(x) = (2/\sqrt{\pi}) \int_x^\infty e^{-t^2} dt$.

Let N_{TM} be the number of available transmission modes. The entire SNR domain is divided into $N_{TM} + 1$ non-overlapping consecutive intervals, with boundary points denoted by $[\gamma_n, \gamma_{n+1})$ where $0 \leq n \leq N_{TM}$. Transmission mode n is selected when $\gamma \in [\gamma_n, \gamma_{n+1})$. To avoid transmission in deep channel fading, no data is sent when $\gamma \in [\gamma_0, \gamma_1)$. That is, in mode $n = 0$, $R_0 = 0$. We will determine the boundary points $\gamma_n, 0 \leq n \leq N_{TM} + 1$. We can derive the

Algorithm 2 Finding $\{\gamma_n\}, 0 \leq n \leq N_{TM} + 1$.

01. $n := N_{TM}$
02. $\gamma_{N_{TM}+1} := +\infty$
03. **while** $n > 1$ **do**
04. Use Eq. (6) to find γ_n such that $\bar{P}_b(n) = P'_b$
05. $n = n - 1$
06. **end while**
07. $\gamma_0 = 0$

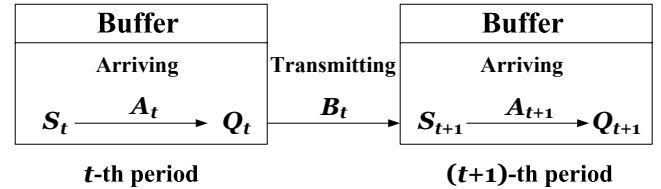
 Fig. 6. The pseudo code used to find $\{\gamma_n\}, 0 \leq n \leq N_{TM} + 1$.


Fig. 7. Diagram of the evolution of queue states.

probability that transmission mode n , denoted by $\Pr\{n\}$, is selected as follows:

$$\Pr\{n\} = \int_{\gamma_n}^{\gamma_{n+1}} p_\gamma(\gamma) d\gamma \\ = \frac{1}{\Gamma(m)} \left[\Gamma \left(m, \frac{m\gamma_n}{\bar{\gamma}} \right) - \Gamma \left(m, \frac{m\gamma_{n+1}}{\bar{\gamma}} \right) \right], \quad (4)$$

where $n = 0, 1, 2, \dots, N_{TM}$ and $\Gamma(a, z)$ is the upper incomplete Gamma function which is defined as:

$$\Gamma(a, z) \triangleq \int_z^\infty t^{a-1} e^{-t} dt. \quad (5)$$

Let $\bar{P}_b(n)$ be the average BER corresponding to transmission mode n :

$$\bar{P}_b(n) = \frac{1}{\Pr\{n\}} \int_{\gamma_n}^{\gamma_{n+1}} P_b^{I,J}(\gamma) p_\gamma(\gamma) d\gamma. \quad (6)$$

We develop Algorithm 2, as shown in Fig. 6, to find the thresholds $\{\gamma_n\}$ such that the predetermined P'_b can be achieved for each transmission mode, i.e., $\bar{P}_b(n) \leq P'_b$.

B. The Queuing Model

We then develop the queuing model to analyze the performance of our proposed schemes, in terms of the idle probability of time slots, packet drop rate, throughput, head of line delay, and average packet delay.

Let t ($t = 0, 1, 2, \dots$) index the frame periods, each of which has a length of T . Denote by S_t and Q_t the queue lengths of the buffer at the beginning and the end of the t -th frame period, respectively. Let K be the buffer capacity in terms of packets. It is clear that the evolution of queue states can be characterized by Q_t with $0 \leq Q_t \leq K$, as shown in Fig. 7.

Let A_t be the number of arrival packets during t -th frame period. The stochastic process of the packet arrival $\{A_t\}$ is stationary and independent of the queue states and the channel states. Also, if we denote by λ the packet arrival rate per node, then $E[A_t] = \lambda T$. On one hand, if we assume that the packet arrival process A_t is a Poisson process with a packet arrival

rate of λ , then we have the probability mass function (pmf) of A_t as follows:

$$\Pr\{A_t = a\} = \begin{cases} \frac{(\lambda T)^a e^{-\lambda T}}{a!}, & a \geq 0 \\ 0, & a < 0. \end{cases} \quad (7)$$

On the other hand, for the case of constant arrival process, the pmf of A_t can be written as follows:

$$\Pr\{A_t = a\} = \begin{cases} 1, & a = \lambda T \\ 0, & \text{otherwise.} \end{cases} \quad (8)$$

Suppose that each packet has a constant payload of p bytes. Denote by B_t the random variable for the number of transmitted packets during the t -th frame period. The transmission mode of the adaptive modulation module during the t -th frame period decides the value of B_t . Denote R_s and R_n as the symbol rates for each transmission mode and the number of bits per symbol in transmission mode n , respectively. Thus, given transmission mode n during t -th frame period, the number of transmitted packets is $B_t = \lfloor R_s R_n T_s / (h + p) \rfloor$. Note that the sensor nodes send packets at a constant power. Since the transmission mode depends on the received SNR γ , which follows Nakagami- m distribution, we obtain the pmf of B_t as follows:

$$\Pr\left\{B_t = \left\lfloor \frac{R_s R_n T_s}{h + p} \right\rfloor\right\} = \Pr\{n\}, \quad (9)$$

where $\Pr\{n\}$ is given in Eq. (4), T_s is the length of a time slot, p and h are the packet payload and overhead, respectively, and $\gamma_n, n = 0, 1, \dots, N_{TM} + 1$, is determined by Algorithm 2.

Define S_{t+1} as the number of packets in the buffer at the beginning of $(t + 1)$ -th frame period. According to our proposed protocols, S_{t+1} is dependent of Q_t and B_t . In particular, we derive S_{t+1} as follows:

$$S_{t+1} = \max\{0, Q_t - \delta_t B_t\}, \quad (10)$$

where

$$\delta_t = \begin{cases} 0, & (Q_t < \theta_b) \vee ((B_t < \theta_a) \wedge (Q_t < \theta_c)) \\ 1, & \text{otherwise} \end{cases} \quad (11)$$

with $1 \leq \theta_a, \theta_b, \theta_c \leq K$ and $\theta_c > \max\{\theta_a, \theta_b\}$. Here, θ_a, θ_b and θ_c are predefined parameters. In fact, δ_t indicates whether packets will be transmitted or not based on the current channel and queue states.

Since the conditional probability that there are s packets in the buffer at the beginning of $(t + 1)$ -th frame period, given that the buffer already has r packets at the end of t -th frame period, depends on the number of packets transmitted during t -th frame period, we have

$$\Pr\{S_{t+1} = s | Q_t = r\} = \begin{cases} \Pr\{B_t = r - s\}, & \{[(\theta_b \leq r < \theta_c) \wedge (r - s \geq \theta_a)] \\ & \vee (r \geq \theta_c)\} \wedge (s > 0) \\ \sum_{b=r}^{\infty} \Pr\{B_t = b\}, & \{[(\theta_b \leq r < \theta_c) \wedge (r - s \geq \theta_a)] \\ & \vee (r \geq \theta_c)\} \wedge (s = 0) \\ \Pr\{B_t < \theta_a\}, & \max\{\theta_a, \theta_b\} \leq r = s < \theta_c \\ 1, & r = s < \max\{\theta_a, \theta_b\} \\ 0, & \text{otherwise.} \end{cases} \quad (12)$$

The queue length of buffer during the $(t + 1)$ -th frame period is $Q_{t+1} = \max\{K, S_{t+1} + A_{t+1}\}$. Then, given $S_{t+1} = s$, the conditional pmf of Q_{t+1} can be expressed as follows:

$$\Pr\{Q_{t+1} = q | S_{t+1} = s\} = \begin{cases} \Pr\{A_{t+1} = q - s\}, & (s \leq q) \wedge (q < K) \\ \sum_{a=q-s}^{\infty} \Pr\{A_{t+1} = a\}, & (s < q) \wedge (q = K) \\ 1, & s = q = K \\ 0, & \text{otherwise.} \end{cases} \quad (13)$$

For simplicity of presentation, we define the following probabilities:

$$\begin{cases} \alpha_{q,s} \triangleq \Pr\{Q_{t+1} = q | S_{t+1} = s\} \\ \beta_{s,r} \triangleq \Pr\{S_{t+1} = s | Q_t = r\}. \end{cases} \quad (14)$$

Then, we can obtain the transition probability, denoted by $P_{q,r}$, that there are q packets in the buffer given that the queue length is r at the previous frame period, as follows:

$$\begin{aligned} P_{q,r} &\triangleq \Pr\{Q_{t+1} = q | Q_t = r\} \\ &= \sum_{s=0}^K \Pr\{Q_{t+1} = q | S_{t+1} = s, Q_t = r\} \\ &\quad \times \Pr\{S_{t+1} = s | Q_t = r\} \\ &\stackrel{(a)}{=} \sum_{s=0}^K \Pr\{Q_{t+1} = q | S_{t+1} = s\} \Pr\{S_{t+1} = s | Q_t = r\} \\ &= \sum_{s=0}^K \alpha_{q,s} \beta_{s,r} \end{aligned} \quad (15)$$

where the equation of (a) holds because the number of packets in buffer at the end of $(t + 1)$ -th frame period depends only on the number of packets at the beginning of $(t + 1)$ -th frame period and the number of packets arrived during $(t + 1)$ -th frame period. Note that $\{Q_t\}$ can be modeled as a finite state Markov chain (FSMC). We then construct the probability transition matrix $\mathbf{P} = \{P_{q,r}\}_{(K+1) \times (K+1)}$. It is clear that the stationary distribution of the FSMC $\{Q_t\}$ exists and is unique. Denote by π_n the stationary pmf of the number of packets in the buffer at the end of a frame period, i.e.,

$$\pi_n \triangleq \lim_{t \rightarrow \infty} \Pr\{Q_t = n\}, \quad (16)$$

where $0 \leq n \leq K$.

The stationary pmf π_n satisfies the following equations:

$$\begin{cases} \sum_{n=0}^K \pi_n = 1 \\ \mathbf{\Pi} = \mathbf{P}\mathbf{\Pi} \end{cases}, \quad (17)$$

where $\mathbf{\Pi}$ is the column vector of π_n and is given by

$$\mathbf{\Pi} \triangleq (\pi_0, \pi_1, \dots, \pi_K)^T, \quad (18)$$

and $(\cdot)^T$ denotes transpose.

After obtaining π_n , we therefore use Eq. (12) to obtain the stationary pmf, denoted by σ_n , of the number of packets at the beginning of a frame period, i.e.,

$$\begin{aligned} \sigma_n &= \lim_{t \rightarrow \infty} \Pr\{S_t = n\} = \lim_{t \rightarrow \infty} \sum_{r=0}^K \Pr\{S_{t+1} = n | Q_t = r\} \pi_r \\ &= \sum_{r=0}^K \beta_{n,r} \pi_r. \end{aligned} \quad (19)$$

C. Performance Metrics

We then derive the five performance metrics including: the packet drop rate, the idle probability of time slots, the average packet delay, the head-of-line (HOL) delay index, and the throughput based on the queuing model, which are detailed, respectively, as follows.

(i) The Packet Drop Rate

If we denote by L_t the number of dropped packets due to the buffer overflow during t -th frame period, then we obtain

$$L_t = \max\{0, A_t - (K - S_t)\}. \quad (20)$$

So, we can derive the pmf of L_t as follows:

$$\Pr\{L_t = n\} = \begin{cases} \sum_{s=0}^K \sum_{m=0}^{K-s} \Pr\{A_t = m\} \Pr\{S_t = s\}, & n = 0 \\ \sum_{s=0}^K \Pr\{A_t = n + K - s\} \Pr\{S_t = s\}, & n > 0. \end{cases} \quad (21)$$

Then, we get the packet dropping rate, denoted by ω , in the steady state, which is equal to the ratio of the average number of dropped packets to the average number of arrival packets during a frame period, as follows:

$$\omega = \lim_{t \rightarrow \infty} \frac{E[L_t]}{E[A_t]} = \frac{\sum_{n=1}^{\infty} \sum_{s=0}^K n \sigma_s \Pr\{A_t = n + K - s\}}{\lambda T}. \quad (22)$$

(ii) The Idle Probability of Time Slots

Next, we calculate the idle probability, denoted by ϕ , that a time slot is not used by the sensor node in the steady state. The idle probability is equivalent to the probability that the number of packets in the buffer at the end of the current frame period is equal to that at the beginning of the next frame period, i.e.,

$$\phi = \sum_{n=0}^K \Pr\{S_{t+1} = n, Q_t = n\} = \sum_{n=0}^K \beta_{n,n} \pi_n. \quad (23)$$

where $\beta_{n,n}$ is given by Eq. (14). It is worth noting that the higher the idle probability of time slots, the larger the chance that the batteries can recover.

(iii) The Head-of-Line (HOL) Delay

To study the packet waiting time in the worst case, we introduce the HOL delay, denoted by D , which is defined as the duration in terms of the frame period from the time when a packet arrives at the head of packet queue in the buffer to the time when the packet leaves the buffer in the steady state. We obtain the pmf of HOL delay as follows:

$$\Pr\{D = d\} = \begin{cases} \sum_{q_0, q_1, \dots, q_d=1}^K \pi_{q_0} \left(\sum_{i=0}^{q_d-1} \beta_{i, q_d} \right) \prod_{j=0}^{d-1} \alpha_{q_{j+1}, q_j} \beta_{q_j, q_j}, & d > 0 \\ \pi_0 + \sum_{n=1}^K \sum_{i=0}^{n-1} \pi_n \beta_{i,n}, & d = 0 \end{cases} \quad (24)$$

where the HOL delay D can take $d = 1, 2, 3, \dots$. The derivation of Eq. (24) is detailed in Appendix A. We then denote the HOL delay index as the probability that the duration when packet stays in the buffer after it arrives at the head of queue is larger than one frame period, i.e., $\Pr\{D > 1\}$. The

larger the HOL delay index is, the longer the HOL packets are delayed on average.

(iv) The Average Packet Delay

For the case of Poisson packet arrival process, if we denote by ν_n the probability that there are n packets in the queue at any random epoch, then the pmf ν_n of queue length at any random epoch can be obtained by

$$\nu_n = \begin{cases} \sum_{s=0}^K \frac{\sigma_s}{\lambda T} \left(1 - \frac{\Gamma(n-s+1, \lambda T)}{(n-s)!} \right), & 0 < n < K \\ \sum_{s=0}^K \sum_{j=K-s}^{\infty} \frac{\sigma_s}{\lambda T} \left(1 - \frac{\Gamma(j+1, \lambda T)}{j!} \right), & n = K \end{cases} \quad (25)$$

where $\Gamma(a, z)$ is the upper incomplete Gamma function. The derivation of Eq. (25) is detailed in Appendix B. We can obtain the average number of buffered packets, denoted by \bar{N} , at any random epoch as follows:

$$\bar{N} = \sum_{n=0}^K n \nu_n. \quad (26)$$

Applying the Little's formula, we obtain the average packet delay, denoted by \bar{W}_q , as following:

$$\bar{W}_q = \frac{\bar{N}}{\lambda(1-\omega)}. \quad (27)$$

On the other hand, in the constant packet arrival case, we get the average packet delay, which is given by

$$\bar{W}_q = \frac{\sum_{n=0}^K n (\pi_n - \frac{\lambda T}{2})}{\lambda(1-\omega)}. \quad (28)$$

(v) The Throughput

Since the packet that enters the buffer can be eventually sent to the coordinators, the throughput, denoted by η , can be obtained by

$$\eta = 8(p+h)\lambda(1-\omega) \quad (29)$$

where p and h are the packet payload and packet overhead, respectively, in bytes, and ω is the packet drop rate given by Eq. (22).

VI. PERFORMANCE EVALUATIONS

The parameters used to evaluate our proposed battery-aware TDMA based MAC protocols are listed in Table I. To satisfy different QoS requirements in terms of packet drop rate and average packet delay, we adopt different combinations of θ_a , θ_b , and θ_c . Clearly, the larger θ_a , θ_b , and θ_c , the poorer delay-QoS performance our proposed schemes can achieve, and also the longer battery lifespan for the sensor nodes can achieve. In this paper, $(\theta_a, \theta_b, \theta_c)$ is set to $(1, 1, 2)$, $(1, 2, 5)$, $(3, 3, 15)$, $(3, 4, 20)$, and $(4, 5, 20)$ for different cases in the order of lower to higher delay-QoS requirements. Note that when $(\theta_a, \theta_b, \theta_c) = (1, 1, 2)$, it corresponds to the standard TDMA scheduling scheme. Also, the schemes with $(1, 2, 5)$, $(3, 3, 15)$, $(3, 4, 20)$, and $(4, 5, 20)$ are referred to as **Scheme-I**, **Scheme-II**, **Scheme-III**, and **Scheme-IV**, respectively, in the rest of this paper.

We develop a customized event-driven simulator that includes the battery discharge model to simulate our proposed schemes in various scenarios where the packet arrival rate per node (λ) varies. In the adaptive modulation module, there

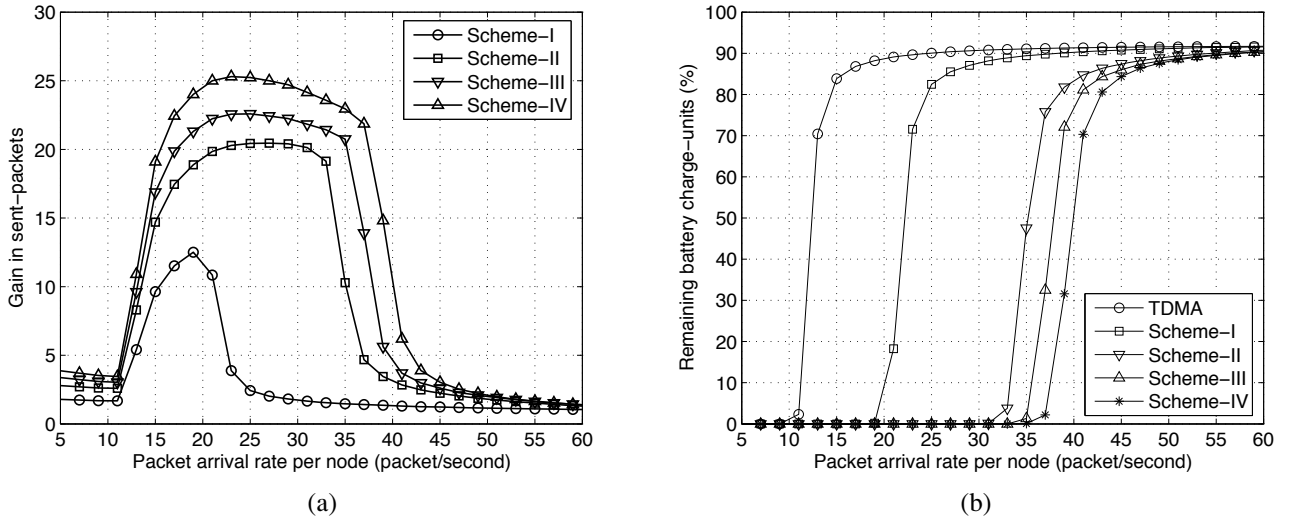


Fig. 8. Simulation results on battery lifetime for standard TDMA scheme and **scheme-I** through **Scheme-IV**. (a) Performance gain over the standard TDMA in terms of the total number of packets sent before the battery dies against the packet arrival rate when $c = 0.01$. (b) The remaining battery capacity in terms of charge-units against the packet arrival rate when $c = 0.01$.

TABLE I
PARAMETERS USED IN THE PROTOCOL PERFORMANCE EVALUATIONS.

T	Frame period	50 ms
T_s	Length of a time slot	2 ms
R_s	Symbol rate	256 ks/s
p	Packet payload	40 bytes
h	Packet overhead	20 bytes
K	Buffer size in packet	25
m	Nakagami parameter	1
E_T	Theoretically capacity of the battery	2500 charge units
E_N	Nominal capacity of the battery	200 charge units
P'_b	Predetermined BER	10^{-5}
$\bar{\gamma}$	Average SNR at the receiver side	25 dB

are six transmission modes. The modulations for transmission modes 1 to 6 are BPSK, QPSK, 8-QAM, 16-QAM, 32-QAM, and 64-QAM, respectively. As a result, $R_n = n$ with $1 \leq n \leq 6$. We use Algorithm 2, as shown in Fig. 6, to determine the required SNR threshold for each transmission mode. For each scenario we run the simulations for 500 times with different initial random seeds to obtain the mean value as the final performance metric.

A. The Case of Poisson Packet Arrival

We first analyze the case where packets arrive according to Poisson process. Fig. 8 shows the simulation results on battery lifetime when the battery recovery ability (c) is set to 0.01. Fig. 8(a) depicts the ratio of the total number of packets sent by our proposed schemes until the battery dies to that by the standard TDMA scheme. From Fig. 8(a), we observe that our proposed schemes, especially **Scheme-IV**, can send more packets than the standard TDMA scheme regardless of the packet arrival rate. For example, the total number of packets sent by **Scheme-IV** can be 25 times as many as that sent by the standard TDMA scheme when the packet arrival rate per node is 22.5. Fig. 8(b) shows the remaining battery capacity in terms of charge-units at the end of the simulation against the packet arrival rate. The less remaining battery capacity

indicates that the battery is used more thoroughly, and thus more packets can be sent. **Scheme-IV** has the least remaining battery capacity among the three schemes because **Scheme-IV** enables the most idle time for the battery to recover the charge-units. The **Scheme-I** has the remaining battery capacity in between.

Figures 9(a), (b), (c), and (d) show the analytical and simulation results of average packet delay, idle probability of time slots, average packet drop rate, and HOL delay index, respectively. It is worth noting that the simulation and analytical results agree well. As shown in Fig. 9(a), the average packet delay of **Schemes I-IV** decreases when the packet arrival rate per node increases from 5 to 25. However, as the packet arrival rate per node keeps increasing, the average packet delay of **Schemes I-IV** increases. On the other hand, the average packet delay of standard TDMA monotonically increases as the packet arrival rate per node increases. The reason behind this can be found in Fig. 9(d) where the HOL delay index is shown. The larger the HOL delay index, the larger the probability that the HOL packets need to take more time to wait in the buffer. From Fig. 9(d), the HOL delay index is zero for the standard TDMA case regardless of packet arrival rate per node because standard TDMA scheme transmits the buffered packets whenever the transmission time slot arrives. At the same time, the HOL delay index of **Schemes I-IV** monotonically decreases as the packet arrival rate per node increases. This is expected because under **Schemes I-IV** the HOL packets have to wait for enough packets in the buffer before they can be transmitted. The lower packet arrival rate per node implies the longer waiting time for the HOL packets. From Fig. 9(a), we observe that the average packet delay of **Scheme-IV** decreases when the packet arrival rate per node is larger than 55. The decrease of average packet delay is caused by the dramatic increase of packet drop rate, which can be observed in Fig. 9(c).

As shown in Fig. 9(b), when the packet arrival rate per node increases, the idle probability of time slots decreases

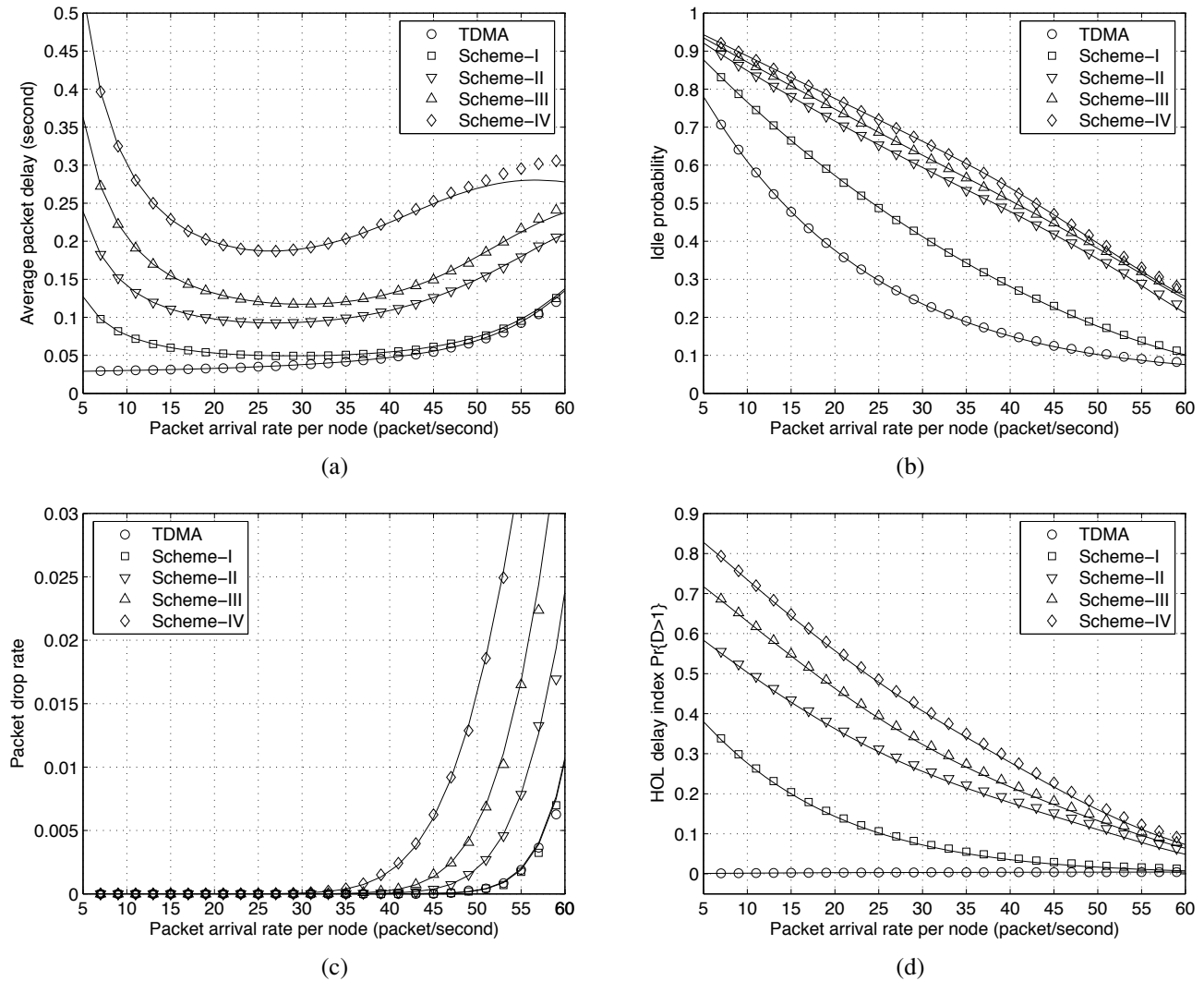


Fig. 9. Different performance metrics against the packet arrival rate when $c = 0.01$ for various schemes. (a) Average packet delay. (b) Idle probability of time slots. (c) Average packet drop rate. (d) HOL delay index ($\Pr\{D > 1\}$). The plots with different symbols denote the simulation results for different schemes and the line plots denote the various analytical results for different simulated schemes illustrated by the corresponding symbol plots.

for any given schemes. In **Scheme-IV**, the idle probability of time slots is the largest given any specific packet arrival rate. The larger the idle probability of time slots, the more the times that the battery has chances to recover. This is the important reason why among all schemes the **Scheme-IV** can use the battery most thoroughly as already observed in Fig. 8(b). From Fig. 9(c), we observe that the average packet drop rate increases as the packet arrival rate gets larger. The average packet drop rates achieved by **Scheme-I** and standard TDMA scheme, respectively, are very close. Before the packet arrival rate reaches 30 packets per second, the average packet drop rates achieved by the five schemes are close to 0.

B. Example Study of Constant Packet Arrival Case: ECG Monitoring Application

Based on the above observations, we find that there exist tradeoffs among the battery lifespan, the packet delay, and the packet drop rate for either the Poisson packet arrival case or the constant packet arrival case. In the practical case, we can select different scheme parameters ($\theta_a, \theta_b, \theta_c$) to satisfy different QoS requirements of various applications.

For example, in the scenario where the power saving is the first priority while packet delay and packet drop rate are less important, we can choose larger θ_a, θ_b , and θ_c (e.g., **Scheme-III** or **Scheme-IV**). Otherwise, we can use smaller θ_a, θ_b , and θ_c (e.g., **Scheme-I**).

We then take the ECG monitoring application as the example to demonstrate the selection of parameters for our proposed schemes. Each sensor node is embedded with a ECG lead which generates signal samples at a constant rate. The number of sensors varies from 2 to 16. The size of each sample is set to 2 bytes. The sample per lead per second is set to 200 and 400, which results in the packet arrival rate per node being 10 and 20, respectively. For the medical application of myoelectric prosthesis control, the ECG delay should be less than 300 ms [15]. IEEE 802.15.4 protocol with CAP mode [6] and Bluetooth with piconet mode are also simulated and compared with our proposed scheme. The parameters for the IEEE 802.15.4 are setting as follows: $macBeaconOrder = 2$, $macSuperframeOrder = 2$, operation band is set to 2.4 GHz, data rate is 250 kb/s. For the Bluetooth with piconet mode, A coordinator (i.e., master device) and multiple sensor

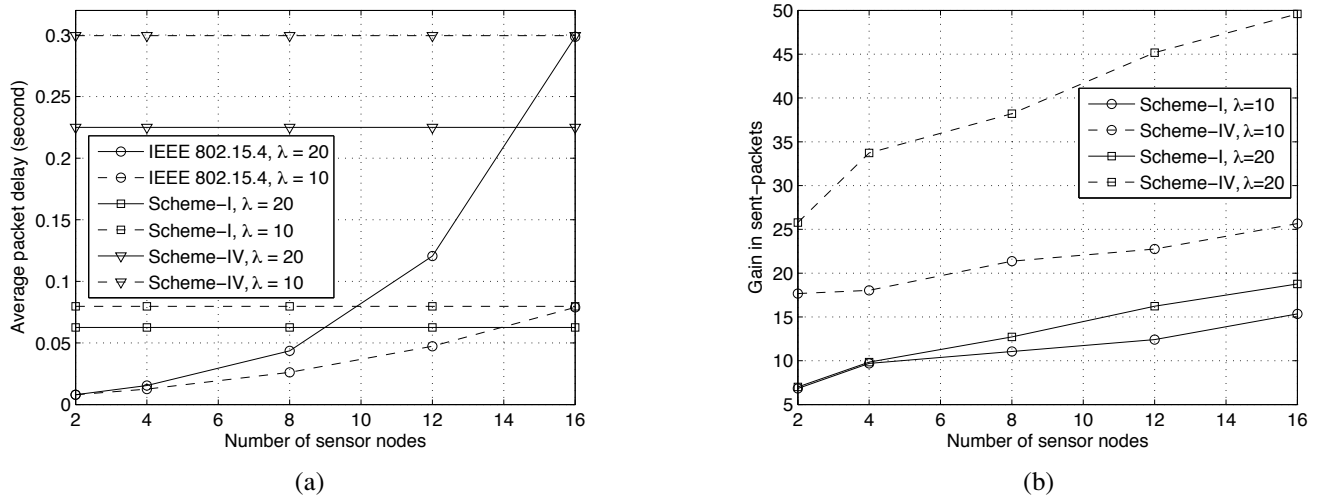


Fig. 10. Performance comparison between our proposed schemes and the IEEE 802.15.4. (a) Average packet delay against the number of sensor nodes. (b) Performance gain of our proposed schemes in terms of number of sent packets over the IEEE 802.15.4.

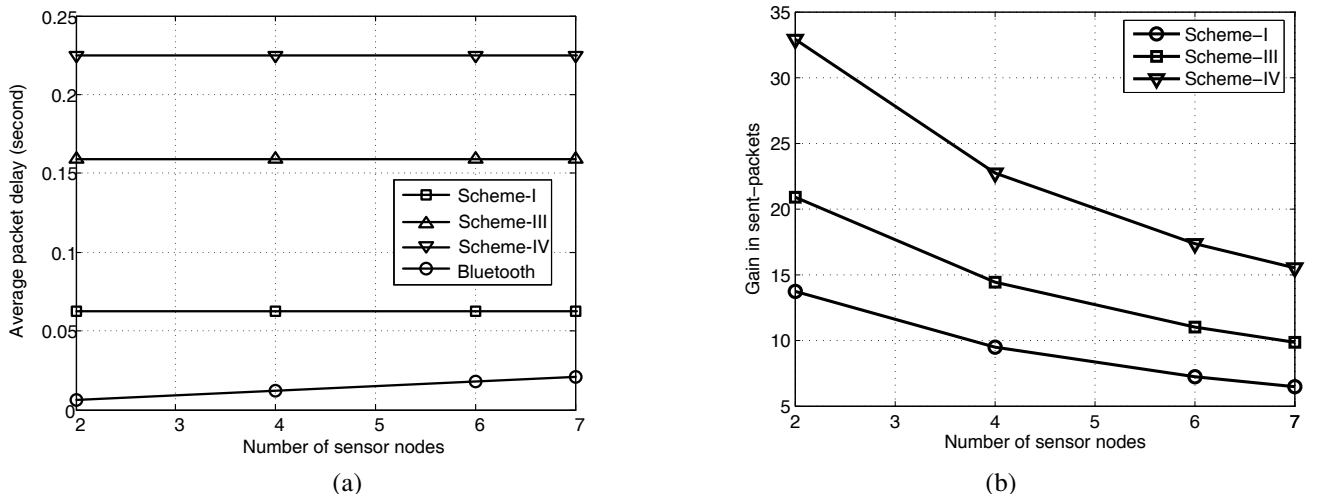


Fig. 11. Performance comparison between our proposed schemes and the Bluetooth protocol. (a) Average packet delay against the number of sensor nodes. (b) Performance gain of our proposed schemes in terms of number of sent packets over the Bluetooth protocol.

nodes (i.e., slave devices) form the master/slave pico-network based on TDMA scheduling. At most 7 sensor nodes are supported in the piconet mode.

Figure 10 shows the performance comparison among our **Scheme-I**, **Scheme-IV** and IEEE 802.15.4 when the number of sensor nodes changes from 2 to 16. As shown in Fig. 10(a), when the packet arrival rate per node is 10, both the average packet delays of **Scheme-I** and **Scheme-IV** are less than 300 ms, which implies that both schemes are applicable for the ECG monitoring application. However, when the packet arrival rate per node is 20, the average packet delay of **Scheme-IV** is highly close to 300 ms, which makes it not suitable for the application. As shown in Fig. 10(a), the average packet delay achieved by either **Scheme-I** or **Scheme-IV** is a constant regardless of the number of sensor nodes. As long as there are enough time slots for the sensors, the constant packet delay can be guaranteed in our TDMA-based schemes. On the other hand, the average packet delay of IEEE 802.15.4 is not upper-bounded and grows with the number of sensor nodes. In IEEE 802.15.4 CAP mode, the larger number of nodes causes the

more packet collisions, resulting in the larger packet delay.

Figure 10(b) shows the performance gain of our schemes over IEEE 802.15.4 in terms of number of sent packets before battery dies. As the number of sensor nodes increases, the gains of **Scheme-I** and **Scheme-IV** get larger. Given the same number of sensor nodes, the gain in sent-packets becomes larger when the packet arrival rate per node changes from 10 to 20. Overall, **Scheme-IV** can send the most packets before battery dies compared to the other two schemes. As shown in Fig. 10(b), when the number of sensor nodes is 16 and the packet arrival rate per node is 10, the number of packets sent by **Scheme-IV** is 26 times as many as that sent by IEEE 802.15.4. The reason why our proposed schemes can send more packets than the IEEE 802.15.4 is because under the IEEE 802.15.4 the sensor nodes spend extra energy on channel detection and packet collisions, which however are avoided in our TDMA-based schemes.

The performance comparison between the Bluetooth and our proposed schemes is given in Fig. 11 when the packet arrival rate is 20 packets per second. As shown in Fig. 11(a),

$$\begin{aligned}
\Pr\{D = d\} &= \Pr\{(Q_t = S_{t+1}) \wedge (Q_{t+1} = S_{t+2}) \wedge (Q_{t+2} = Q_{t+3}) \cdots \wedge (Q_{t+d-1} = S_{t+d}) \wedge (Q_{t+d} \neq S_{t+d+1})\} \\
&= \sum_{q_0, q_1, q_2, \dots, q_d=1}^K \Pr\{Q_t = q_0, S_{t+1} = q_0, Q_{t+1} = q_1, S_{t+2} = q_1, Q_{t+2} = q_2, S_{t+3} = q_2, \dots, \\
&\quad Q_{t+d-1} = q_{d-1}, S_{t+d} = q_{d-1}, Q_{t+d} = q_d, S_{t+d+1} < q_d\} \\
&= \sum_{q_0, q_1, q_2, \dots, q_d=1}^K \pi_{q_0} \Pr\{Q_{t+1} = q_1, S_{t+1} = q_0 | Q_t = q_0\} \Pr\{Q_{t+2} = q_2, S_{t+2} = q_1 | Q_{t+1} = q_1\} \\
&\quad \cdots \times \Pr\{Q_{t+d} = q_d, S_{t+d} = q_{d-1} | Q_{t+d-1} = q_{d-1}\} \Pr\{S_{t+d+1} < q_d | Q_{t+d} = q_d\} \\
&= \sum_{q_0, q_1, q_2, \dots, q_d=1}^K \pi_{q_0} (\alpha_{q_1, q_0} \beta_{q_0, q_0}) \cdots (\alpha_{q_d, q_{d-1}} \beta_{q_{d-1}, q_{d-1}}) \left(\sum_{i=0}^{q_d-1} \beta_{i, q_d} \right) \\
&= \sum_{q_0, q_1, q_2, \dots, q_d=1}^K \pi_{q_0} \left(\sum_{i=0}^{q_d-1} \beta_{i, q_d} \right) \prod_{j=0}^{d-1} \alpha_{q_{j+1}, q_j} \beta_{q_j, q_j} \tag{33}
\end{aligned}$$

the average packet delay is constant for our proposed schemes. For the Bluetooth protocol, the average packet delay increases with the number of sensor nodes. This is because the period of frame for the Bluetooth protocol increases with the number of participated sensor nodes, which leads to the increase of average packet delay. The average packet delay achieved by Bluetooth is less than that achieved by our proposed schemes. It is expected since the Bluetooth protocol can be considered as the standard TDMA scheme, which can provide the stringent QoS-delay requirements.

Figure 11(b) shows the performance gain of our schemes over the Bluetooth in terms of number of sent packets before battery dies. Our proposed schemes outperform the Bluetooth protocol. For example, the number of packets sent by **Scheme-IV** is 34 times as many as that sent by Bluetooth during the battery lifetime when the number of sensor nodes is 2. It is because the sensor nodes are active during each frame period in the Bluetooth, which causes the batteries to have much less rest period to recover as compared with **Scheme-IV**. As the number of sensor nodes increases, the gains of **Scheme-I**, **Scheme-III**, and **Scheme-IV** get smaller. This is because when the number of sensor nodes increases, each sensor node can have longer idle period to recover the battery capacity under the Bluetooth protocol.

VII. CONCLUSIONS

We proposed and analyzed the cross-layer based battery-aware TDMA MAC protocols for wireless monitoring networks in wireless healthcare applications. The development of our proposed schemes is based on the cross-layer design technique, which takes battery recovery dynamics, time-varying wireless channels at the physical layer, and queuing management at the data link layer into account. We developed a discrete time Markov chain based analytical model to study the performance of our proposed schemes. Simulations were conducted to validate our analytical model. The analytical and simulation results show that our proposed schemes can highly increase the battery lifespan while satisfying the delay QoS requirements for the wireless body-area monitoring networks.

APPENDIX

A. THE DERIVATION OF EQ. (24)

We first derive the conditional probability given $Q_t = n$, $S_{t+1} = Q_t$ and $Q_{t+1} = m$ in the steady state as follows:

$$\begin{aligned}
&\Pr\{Q_{t+1} = m, S_{t+1} = n | Q_t = n\} \\
&= \Pr\{Q_{t+1} = m | Q_t = n, S_{t+1} = n\} \Pr\{S_{t+1} = n | Q_t = n\} \\
&= \alpha_{m,n} \beta_{n,n}. \tag{30}
\end{aligned}$$

The probability that given $Q_t = n$, at least one packet is transmitted during t -th frame period and there are m packets at the end of $(t+1)$ -th frame period is given by

$$\begin{aligned}
&\Pr\{Q_{t+1} = m, S_{t+1} < n | Q_t = n\} \\
&= \sum_{i=0}^{n-1} \Pr\{Q_{t+1} = m, S_{t+1} = i | Q_t = n\} \\
&= \sum_{i=0}^{n-1} \Pr\{Q_{t+1} = m | S_{t+1} = i\} \Pr\{S_{t+1} = i | Q_t = n\} \\
&= \sum_{i=0}^{n-1} \alpha_{m,i} \beta_{i,n}. \tag{31}
\end{aligned}$$

The probability that the HOL delay index D is equal to d in the steady state is equivalent to the probability that no packet is transmitted for exact d consecutive times. If $d = 0$, we have

$$\begin{aligned}
\Pr\{D = 0\} &= \Pr\{Q_t = 0 \vee (Q_t > 0 \wedge Q_t \neq S_{t+1})\} \\
&= \pi_0 + \sum_{n=1}^K \sum_{i=0}^{n-1} \pi_n \beta_{i,n}. \tag{32}
\end{aligned}$$

On the other hand, for $d > 0$, $\Pr\{D = d\}$ is obtained by Eq. (33), which together with Eq. (32) yields Eq. (24).

B. THE DERIVATION OF EQ. (25)

It is a well-known fact that in models where the arrivals follow a Poisson process, the queue state as seen by an arriving packet is the same as for an outside observer (random epoch). Denote by N_t^τ the number of packets during the $tT + \tau$ epoch where $0 \leq \tau \leq T$. Given that there are s packets at the beginning of t -th frame period, the probability that $N_t^\tau = n$ is equal to the probability that there are $(n-s)$ packets arriving

during time-length τ . Then, we obtain

$$\Pr\{N_t^\tau = n | S_t = s\} = \begin{cases} \frac{(\lambda\tau)^{n-s} e^{-(\lambda\tau)}}{(n-s)!}, & s \leq n < K \\ \sum_{j=K-s}^{\infty} \frac{(\lambda\tau)^j e^{-(\lambda\tau)}}{j!}, & n = K. \end{cases} \quad (34)$$

Let N^τ be the number of packets during the $tT + \tau$ epoch in the steady state. We have

$$\Pr\{N^\tau = n\} = \sum_{s=0}^K \sigma_s \Pr\{N_t^\tau = n | S_t = s\}. \quad (35)$$

Thus, the pmf ν_n of queue length at any random epoch can be obtained by

$$\begin{aligned} \nu_n &= \frac{1}{T} \int_0^T \Pr\{N^\tau = n\} d\tau \\ &= \sum_{s=0}^K \frac{\sigma_s}{T} \int_0^T \Pr\{N_t^\tau = n | S_t = s\} d\tau \\ &= \begin{cases} \sum_{s=0}^K \frac{\sigma_s}{\lambda T} \left(1 - \frac{\Gamma(n-s+1, \lambda T)}{(n-s)!}\right), & 0 < n < K \\ \sum_{s=0}^K \sum_{j=K-s}^{\infty} \frac{\sigma_s}{\lambda T} \left(1 - \frac{\Gamma(j+1, \lambda T)}{j!}\right), & n = K \end{cases} \end{aligned} \quad (36)$$

which completes the derivation of Eq. (25).

REFERENCES

- [1] D. Cypher, N. Chevrollier, N. Montavont, and N. Golmie, "Prevailing over wires in healthcare environments: benefits and challenges," *IEEE Commun. Mag.*, vol. 44, no. 4, pp. 56–63, 2006.
- [2] C. Chiasserini and R. Rao, "Energy efficient battery management," in *Proc. IEEE INFOCOM 2000*, vol. 2, 26–30 March 2000, pp. 396–403.
- [3] S. Jayashree, B. S. Manoj, and C. S. R. Murthy, "On using battery state for medium access control in ad hoc wireless networks," in *Proc. ACM MobiCom'04*, Philadelphia, PA, USA, 2004, pp. 360–373.
- [4] G. Pei and C. Chien, "Low power TDMA in large wireless sensor networks," in *Proc. IEEE MILCOM*, 2001.
- [5] V. Rajendran, K. Obraczka, and J. J. Garcia-Luna-Aceves, "Energy-efficient collision-free medium access control for wireless sensor networks," in *SenSys '03: Proc. 1st international conference on Embedded networked sensor systems*, 2003, pp. 181–192.
- [6] IEEE 802.15.4, *Wireless Medium Access Control (MAC) and Physical Layer (PHY) Specifications for Low-Rate Wireless Personal Area Networks (LR-WPANs)*, IEEE Computer Society, October 2003.
- [7] M. Kohvakka, M. Kuorilehto, M. Hännikäinen, and T. D. Hämäläinen, "Performance analysis of IEEE 802.15.4 and ZigBee for large-scale wireless sensor network applications," in *PE-WASUN '06: Proc. 3rd ACM international workshop on Performance evaluation of wireless ad hoc, sensor and ubiquitous networks*, 2006, pp. 48–57.
- [8] Bluetooth, *Specifications of the Bluetooth System - Ver. 1.1 B*, 2001.
- [9] J. Haartsen, "The bluetooth radio system," *IEEE Personal Commun.*, vol. 7, no. 1, pp. 28–36, 2000.
- [10] C. Chiasserini and R. Rao, "Pulsed battery discharge in communication devices," in *Proc. ACM MobiCom '99*, Seattle, Washington, USA, 1999, pp. 88–95.
- [11] —, "A model for battery pulsed discharge with recovery effect," in *Proc. IEEE WCNC*, 21–24 Sept. 1999, pp. 636–639.
- [12] A. Goldsmith, *Wireless Communications*. Cambridge University Press, 2005.
- [13] S. Cotton and W. Scanlon, "Characterization and modeling of the indoor radio channel at 868 mhz for a mobile bodyworn wireless personal area network," *IEEE Antennas Wireless Propag. Lett.*, vol. 6, pp. 51–55, 2007.
- [14] K. Cho and D. Yoon, "On the general BER expression of one- and two-dimensional amplitude modulations," *IEEE Trans. Commun.*, vol. 50, no. 7, pp. 1074–1080, July 2002.
- [15] P. Zhou, B. Lock, and T. A. Kuiken, "Real time ECG artifact removal for myoelectric prosthesis control," *Physiological Measurement*, vol. 28, pp. 397–413, 2007.



Hang Su (S'04) received B.S. and M.S. degrees in electrical engineering from Zhejiang University, Hangzhou, China, in 2002 and 2005, respectively. He is currently working toward a Ph.D. degree at Department of Electrical and Computer Engineering, Texas A&M University, College Station. He worked as a software engineer with Nokia Research Center, Hangzhou, China, in 2005.

His research interests lie in cognitive radio networks, vehicular ad hoc networks, and wireless sensor networks with emphasis on design and analysis of MAC and routing protocols.



Xi Zhang (S'89-SM'98) received the B.S. and M.S. degrees from Xidian University, Xi'an, China, the M.S. degree from Lehigh University, Bethlehem, PA, all in electrical engineering and computer science, and the Ph.D. degree in electrical engineering and computer science (Electrical Engineering-Systems) from The University of Michigan, Ann Arbor.

He is currently an Associate Professor and the Founding Director of the Networking and Information Systems Laboratory, Department of Electrical and Computer Engineering, Texas A&M University, College Station. He was a Research Fellow with the School of Electrical Engineering, University of Technology, Sydney, Australia, and the Department of Electrical and Computer Engineering, James Cook University, Australia, under a Fellowship from the Chinese National Commission of Education. He worked as a Summer Intern with the Networks and Distributed Systems Research Department, AT&T Bell Laboratories, Murray Hills, NJ, and with AT&T Laboratories Research, Florham Park, NJ, in 1997. He has published more than 140 research papers in the areas of wireless networks and communications systems, mobile computing, network protocol design and modeling, statistical communications, random signal processing, information theory, and control theory and systems.

Prof. Zhang received the U.S. National Science Foundation CAREER Award in 2004 for his research in the areas of mobile wireless and multicast networking and systems. He received the Best Paper Award in the IEEE Globecom 2007. He also received the TEES Select Young Faculty Award for Excellence in Research Performance from the Dwight Look College of Engineering at Texas A&M University, College Station, in 2006. He is currently serving as an Editor for the IEEE TRANSACTIONS ON WIRELESS COMMUNICATIONS, an Associate Editor for the IEEE TRANSACTIONS ON VEHICULAR TECHNOLOGY, a Guest Editor for the IEEE JOURNAL ON SELECTED AREAS IN COMMUNICATIONS for the special issue on "wireless video transmission", an Associate Editor for the IEEE COMMUNICATIONS LETTERS, a Guest Editor for the *IEEE Wireless Communications Magazine* for the special issue on "next generation of CDMA versus OFDMA for 4G wireless applications", an Editor for the JOHN WILEY'S JOURNAL ON WIRELESS COMMUNICATIONS AND MOBILE COMPUTING, an Editor for the JOURNAL OF COMPUTER SYSTEMS, NETWORKING, AND COMMUNICATIONS, and an Associate Editor for the JOHN WILEY'S JOURNAL ON SECURITY AND COMMUNICATIONS NETWORKS, and is also serving as a Guest Editor for JOHN WILEY'S JOURNAL ON WIRELESS COMMUNICATIONS AND MOBILE COMPUTING for the special issue on "next generation wireless communications and mobile computing". He has frequently served as the Panelist on the U.S. National Science Foundation Research-Proposal Review Panels. He is serving or has served as the TPC Vice-Chair for IEEE INFOCOM 2010, TPC Chair for IEEE Globecom 2011, Co-Chair for IEEE INFOCOM 2009 - Mini-Conference, Co-Chair for IEEE Globecom 2008 - Wireless Communications Symposium, Co-Chair for the IEEE ICC 2008 - Information and Network Security Symposium, Symposium Chair for IEEE/ACM International Cross-Layer Optimized Wireless Networks Symposium 2006-2008, the TPC Chair for IEEE/ACM IWCMC 2006-2008, the Poster Chair for IEEE INFOCOM 2008, the Student Travel Grants Co-Chair for IEEE INFOCOM 2007, Executive Committee Co-Chair for ACM QShine. He has served as the TPC members for more than 70 IEEE/ACM conferences, including IEEE INFOCOM, IEEE Globecom, IEEE ICC, IEEE WCNC, IEEE VTC, IEEE/ACM QShine, IEEE WoWMoM, IEEE ICCCN, etc.

Prof. Zhang is a Senior Member of the IEEE and a Member of the Association for Computing Machinery (ACM).